Letter

Turbulent cascade arrests and the formation of intermediate-scale condensates

Kolluru Venkata Kiran [1], Dario Vincenzi [2], and Rahul Pandit [1]

[1] *Centre for Condensed Matter Theory, Department of Physics, Indian Institute of Science, Bangalore 560012, India*

[2] *Université Côte d'Azur, CNRS, LJAD, 06100 Nice, France*

(Received 9 April 2024; accepted 23 August 2024; published 7 October 2024)

Energy cascades lie at the heart of the dynamics of turbulent flows. In a recent study of turbulence in fluids with odd viscosity X. M. de Wit *et al.* [Nature (London) **627**, 515 (2024)], the two dimensionalization of the flow at small scales leads to the arrest of the energy cascade and selection of an intermediate scale, between the forcing and the viscous scales. To demonstrate the generality of the phenomenon and its existence for a wide class of turbulent systems, we study a shell model that is carefully constructed to have three-dimensional turbulent dynamics at small wave numbers and two-dimensional turbulent dynamics at large wave numbers. The large scale separation that we can achieve in our shell model allows us to examine clearly the interplay between these dynamics, which leads to an arrest of the energy cascade at a transitional wave number and an associated accumulation of energy at the same scale. Such pile-up of energy around the transitional wave number is reminiscent of the formation of condensates in two-dimensional turbulence, but, in contrast, it occurs at intermediate wave numbers instead of the smallest wave number.

DOI: 10.1103/PhysRevE.110.L043101

Introduction. Cascade processes are at the origin of the multiscale nature of turbulent flows. The best-known example is Richardson's cascade of kinetic energy in three dimensions (3D) [1]. Energy is injected into a characteristic wave number k_f by an external force that drives the flow. On average, nonlinear interactions transfer the injected energy to larger wave numbers k without dissipation. This process persists up to the Kolmogorov wave number, beyond which viscous dissipation dominates. The continuous interplay between energy injection and viscous dissipation leads to a nonequilibrium statistically stationary state. The direct energy cascade is at the heart of 3D homogeneous isotropic turbulence [1]. In two-dimensional (2D) turbulence, the direction of the energy cascade is reversed and on average energy flows from k_f to smaller values of k; furthermore, the inverse cascade of energy coexists with a direct cascade of enstrophy [2,3]. In general, turbulent cascades of inviscid invariants, and in particular their directions (whether direct or inverse), are affected by phenomena such as rotation, stratification, spatial confinement, and selective suppression of Fourier modes of the velocity [4–7].

Dissipative mechanisms inherent to the system, typically viscous dissipation at large k or frictional dissipation at small k, naturally arrest or suppress a turbulent cascade. However, other complex mechanisms that induce such suppression have been identified in geostrophic [8–10], magnetohydrodynamic [11,12], and bacterial turbulence [13,14]. In particular, de Wit *et al.* [15] recently studied the 3D Navier-Stokes equations (NSE) with an odd-viscosity term that leads to a quasi-two-dimensionalization of the velocity field at large k. If the forcing acts at small k, the direct energy cascade is arrested at an intermediate wave number k_c. Since odd viscous terms are not dissipative, the arrest of the cascade results in an accumulation of energy around k_c and thence an emergence of flow structures of size k_c^{-1}. If the flow is forced at large k, this model displays an inverse energy cascade, which is arrested by the 3D-type behavior of the flow at small k and is accompanied by the formation of structures of intermediate sizes.

We demonstrate that such intermediate-scale cascade arrests are not restricted to odd-viscous fluids but are, in fact, signatures of any turbulent systems where 3D-type dynamics, at small k, coexist with 2D-type dynamics, at large k. To this end, we construct a shell model that can display the desired small- and large-k dynamics. Shell models are a class of hydrodynamical equations, which retain the essential features of the NSE in Fourier space and offer insights into energy-transfer mechanisms in fully developed turbulence [1,16–19]. The interactions between the Fourier modes of the velocity are restricted; thus numerical simulations of shell models reach larger scale separations and better statistical convergence than those presently achievable with direct numerical simulations of the NSE [20]. The tractability of shell models makes them invaluable for studying turbulence. New concepts in turbulence theory that have been recently developed by using shell models include hidden scale invariance [21], subgrid closures [22], stirring strategies for optimizing mixing [23], and the application of avalanche dynamics in amorphous materials in the analysis of the temporal behavior of the kinetic energy [24]. We modify the strategy that was used by Boffetta *et al.* [25] for a shell-model study of thin fluid layers. By allowing the coefficients of the shell model to depend suitably on k, the model captured the split-energy cascade, in quasi-2D turbulent flows, with direct and inverse components [26,27]. We consider scale-dependent coefficients but select them so as to obtain a shell model that is 3D-like at small wave numbers and 2D-like at large wave numbers. The transition between the two cascading regions occurs at a wave number $k_{\rm tr}$; the forcing is localized at the wave number k_f. We find that, irrespective of the ratio of $k_{\rm tr}/k_f$, the reciprocity between the small- and large-wave-number dynamics results in the arrest

of the energy cascade (be it forward or inverse). However, the system dynamics differs depending on whether k_{tr}/k_f is smaller or greater than unity. The main consequence of the arrest of the cascade is a strong buildup of energy close to k_{tr}. We show that a statistically stationary state and the formation of condensates is nevertheless possible because of an increase in viscous dissipation near k_{tr}.

Model. We consider the SABRA shell model [28,29]

$$\frac{du_n}{dt} = i\Phi_n - \left(\mu k_n^{-2} + \nu k_n^2\right)u_n + f_n, \quad 1 \leqslant n \leqslant N, \qquad (1)$$

where $k_n = k_0\lambda^n$, μ and ν are the hyperfriction and viscosity parameters, respectively, and the external forcing, $f_n = \epsilon_f(1+i)\delta_{n,n_f}/2u^*_{n_f}$, injects energy at a constant rate ϵ_f into the shell n_f. The nonlinear term is

$$\Phi_n = a_n k_{n+1}u_{n+2}u^*_{n+1} + b_n k_n u_{n+1}u^*_{n-1} - c_n k_{n-1}u_{n-2}u_{n-1}, \qquad (2)$$

where a_n, b_n, c_n are real and the $*$ denotes complex conjugation. In addition, $u_{-1} = u_0 = u_{N+1} = u_{N+2} = 0$. In the inviscid ($\mu = 0, \nu = 0$) and unforced ($f_n = 0$) case, the total energy $E(t) = \frac{1}{2}\sum_{n=1}^{N}|u_n(t)|^2$ is conserved provided $a_{n-1} + b_n + c_{n+1} = 0$. In the original SABRA model [28], $a_n = a$, $b_n = b$, and $c_n = c$, and $H(t) = \frac{1}{2}\sum_{n=1}^{N}(a/c)^n|u_n(t)|^2$ is a second invariant quantity. Different regimes are observed depending on the ratio c/a. Here, it is sufficient to recall that there is a regime of direct energy cascade, which mimics 3D turbulence, for $-1 < c/a < 0$ [28]. In this regime, H does not have a definite sign and it can be regarded as a generalized helicity. By contrast, H is positive for $0 < c/a < 1$ and in the subrange $\lambda^{-2/3} < c/a < 1$ there is a 2D-turbulence-like regime, with a simultaneous inverse cascade of E and a direct cascade of H. In this case, H plays the role of a generalized enstrophy [29].

To introduce a shell-model analog of the domain aspect ratio in a study of quasi-2D fluid turbulence, Ref. [25] considered a version of the SABRA model with n-dependent coefficients: $\{a_n, b_n, c_n\}$ were chosen to generate an inverse energy cascade for $k_n < k_h$ and a direct energy cascade for $k_n > k_h$, with k_h^{-1} representing the depth of a fluid layer.

We consider a shell model with n-dependent coefficients *but reverse the directions of the energy cascades* by taking

$$a_n = 1, \quad b_n = -0.5, \quad c_n = -0.5, \quad 1 \leqslant n < n_{tr}, \qquad (3)$$

$$a_n = 1, \quad b_n = -1.7, \quad c_n = -0.5, \quad n = n_{tr}, \qquad (4)$$

$$a_n = 1, \quad b_n = -1.7, \quad c_n = 0.7, \quad n_{tr} < n \leqslant N. \qquad (5)$$

Clearly, for modes $n < n_{tr}$ ($n > n_{tr}$) the coefficients $\{a_n, b_n, c_n\}$ lead to a 3D (2D) turbulentlike regime. Note that c_n changes value at n_{tr+1} to respect energy conservation in the inviscid limit.

We investigate the interplay between the small- and large-k_n modes in this model for the cases (a) $k_{tr}/k_f > 1$ and (b) $k_{tr}/k_f < 1$, with $k_{tr} = k_0\lambda^{n_{tr}}$ the transitional wave number. We integrate Eq. (1) by using an Adams-Bashforth scheme [30].

(a) Small-wave-number forcing. We first consider the case $k_f < k_{tr}$ (Table I, runs A and B, in which $\mu = 0$). In the limit $k_{tr}/k_f \to \infty$, we recover the SABRA model with constant 3D-like coefficients. Therefore, in this limit, our model displays a direct cascade of E [28] and the energy flux [$\langle\cdot\rangle$ is the time average]

$$\Pi_E(k_n) = \left\langle \sum_{j=n}^{N} \Re\{i\Phi_j u_j^*\} \right\rangle \qquad (6)$$

is constant and equal to ϵ_f for $k_f \ll k_n \ll k_\nu$, where $k_\nu = (\epsilon_f/\nu^3)^{1/4}$ is the Kolmogorov wave number. In the same range, the energy spectrum $\mathcal{E}(k_n) = \langle|u_n|^2/k_n\rangle$ shows a scaling range that is consistent with $k_n^{-5/3}$, the Kolmogorov (1941) form [1]. For $k_n \ll k_f$, $\mathcal{E}(k_n) \sim k_n^{-1}$, which indicates energy equipartition [5]. Now consider $1 < k_{tr}/k_f \ll \infty$. If $k_{tr} \gtrsim k_\nu$, $E(t)$ does not show significant deviations from the limiting case $k_{tr}/k_f \to \infty$ (inset of Fig. 1). However, when $k_{tr} < k_\nu$ we find that, with decreasing k_{tr} (and fixed k_f), $E(t)$ takes longer to reach the stationary state and its stationary value increases (inset of Fig. 1). To characterize the temporal energy fluctuations $E'(t) = E(t) - \langle E(t)\rangle$ for different k_{tr}, we calculate the time scale τ_c from the exponential decay of the autocorrelation function $C(\tau) = \langle E'(t+\tau)E'(t)\rangle/\langle E'^2(t)\rangle$. Figure 1 shows that τ_c is nearly independent of k_{tr}, for $k_{tr} \geqslant k_\nu$, but it grows rapidly as k_{tr} is decreased below k_ν. These trends are reminiscent of the formation of large-scale condensates in 2D turbulent flows [2,31], where, in the absence of friction, condensate formation is associated with very long saturation times and strong deviations of the energy spectrum from its inertial-range scaling (compare Fig. 2 of Ref. [31] with our Fig. 1). Therefore, we examine the dependence of energy spectra and flux on k_{tr}. In Fig. 2(a), we plot $\Pi_E(k_n)$ [Eq. (6)] for different values of k_{tr}. As long as $k_{tr} > k_\nu$, this flux is indistinguishable from that of the $k_{tr}/k_f \to \infty$ case. However, if $k_{tr} < k_\nu$, $\Pi_E(k_n) \simeq \epsilon_f$ only

TABLE I. Parameters of the shell-model simulations. In addition, $\lambda = 2$, $k_0 = 1/16$, and $\epsilon_f = 5 \times 10^{-3}$ for all runs. The initial condition is $u_n = k_n^{1/2}e^{i\theta_n}$ for $n = 1, 2$ and $u_n = k_n^{1/2}e^{-k_n^2}e^{i\theta_n}$ for $3 \leqslant n \leqslant N$, where θ_n is a random variable distributed uniformly between 0 and 2π.

Run	N	n_f	n_{tr}	ν	μ	δt	k_{tr}/k_ν
A0	28	1	∞	5×10^{-7}	0	1×10^{-4}	∞
A1	28	1	25	5×10^{-7}	0	1×10^{-4}	1.48×10^{2}
A2	28	1	20	5×10^{-7}	0	1×10^{-4}	4.63×10^{0}
A3	28	1	18	5×10^{-7}	0	1×10^{-4}	1.16×10^{0}
A4	28	1	15	5×10^{-7}	0	1×10^{-4}	1.45×10^{-1}
A5	28	1	12	5×10^{-7}	0	1×10^{-4}	1.18×10^{-2}
A6	28	1	10	5×10^{-7}	0	5×10^{-5}	4.50×10^{-3}
B1	28	1	15	1×10^{-7}	0	1×10^{-4}	4.33×10^{-2}
B2	28	1	15	1×10^{-8}	0	1×10^{-5}	7.77×10^{-3}
B3	28	1	15	5×10^{-9}	0	1×10^{-5}	4.60×10^{-3}
C1	34	3	5	1×10^{-10}	1×10^{-3}	1×10^{-4}	2.38×10^{-7}
C2	34	3	7	1×10^{-10}	1×10^{-3}	1×10^{-4}	9.51×10^{-7}
C3	34	3	9	1×10^{-10}	1×10^{-3}	1×10^{-4}	3.80×10^{-7}
D1	34	25	0	1×10^{-10}	5×10^{-4}	1×10^{-5}	0
D2	34	25	15	1×10^{-10}	5×10^{-4}	1×10^{-6}	2.44×10^{-4}
D3	34	25	17	1×10^{-10}	5×10^{-4}	1×10^{-6}	9.74×10^{-4}
D4	34	25	18	1×10^{-10}	5×10^{-4}	1×10^{-6}	1.90×10^{-3}
D5	34	25	20	1×10^{-10}	5×10^{-4}	1×10^{-6}	7.80×10^{-3}

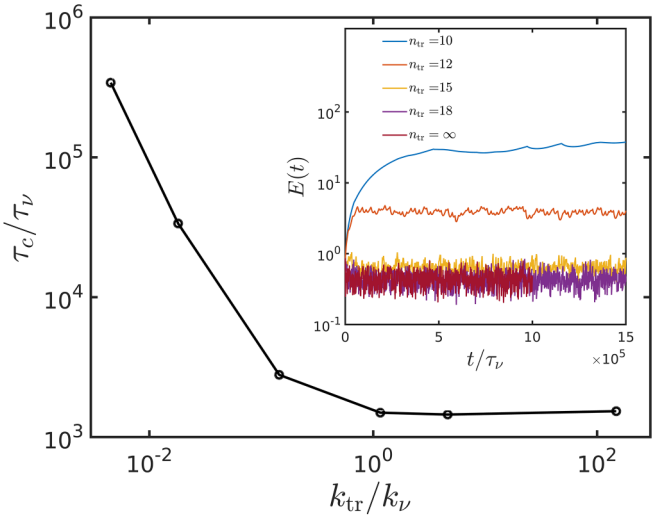

FIG. 1. Plot of the energy-autocorrelation decay time τ_c, scaled by the Kolmogorov time $\tau_\nu = \sqrt{\nu/\epsilon_f}$, as a function of $k_{\rm tr}/k_\nu$. Inset: the time series of the total energy for different values of $n_{\rm tr}$ (runs A0, A3, A4, A5, and A6).

for $k_f < k_n < k_{\rm tr}$, and it vanishes rapidly beyond $k_{\rm tr}$. Thus the direct energy cascade persists up until $k_{\rm tr}$, but is then arrested by the 2D-like dynamics for $k_n > k_{\rm tr}$. The consequence of this arrest is a sharp buildup of energy around $k_{\rm tr}$, as seen in Fig. 2(b), where we plot the compensated energy spectra $k_n^{5/3}\mathcal{E}(k_n)$ versus $k_n/k_{\rm tr}$, for different values of $k_{\rm tr}$. Energy starts accumulating around $k_{\rm tr}$ for $k_{\rm tr} < k_\nu$; this accumulation increases as $k_{\rm tr}$ approaches k_f. We also remark that the suppression of high-frequency fluctuations in $E(t)$, with decreasing $k_{\rm tr}$, is associated with the arrest of the energy cascade at $k_n \approx k_{\rm tr}$.

Despite the buildup of energy at a wavenumber smaller than k_ν, our model reaches a statistically stationary state, albeit at times that increase as $k_{\rm tr}$ decreases. To understand this intriguing behavior, we examine the energy budget in the statistically stationary state:

$$T(k_n) + D_\mu(k_n) + D_\nu(k_n) + F(k_n) = 0. \tag{7}$$

Here, $T(k_n) = \langle \mathrm{Re}\mathrm{i}\{\Phi_n u_n^*\}\rangle$, $F(k_n) = \langle \mathrm{Re}\{f_n u_n^*\}\rangle$, $D_\nu(k_n) = \langle 2\nu k_n^2 |u_n|^2\rangle$, and $D_\mu(k_n) = \langle 2\mu k_n^{-2}|u_n|^2\rangle$ are the nonlinear, forcing, viscous, and friction contributions, respectively. We plot these quantities in the inset of Fig. 2(c) for $n_{\rm tr} = 10$. Since friction is absent, the forcing term is balanced by the transfer term at $k_n = k_f$ and, in the cascade range $k_n < k_{\rm tr}$, the contribution from the transfer term is negligible, so the statistical properties are like those in the pure 3D direct cascade ($k_{\rm tr}/k_f \to \infty$). Deviations from this 3D cascade arise when we account for the dissipation term. The maximum of $|D_\nu(k_n)|$ shifts from $k_n \simeq k_\nu$ to $k_n \simeq k_{\rm tr}$, thus compensating for the accumulation of energy at the same wave numbers. This is clearly shown in the inset of Fig. 2(c), where $T(k_n)$ is balanced by $D_\nu(k_n)$ at $k_n \simeq k_{\rm tr}$. Moreover, as $k_{\rm tr}$ decreases, the maximum of $|D_\nu(k_n)|$ shifts to smaller values of k_n and its magnitude increases to compensate for the stronger buildup of energy [Fig. 2(c)].

In the range $k_n > k_{\rm tr}$, the coefficients in Eq. (3) lead to 2D-like dynamics; hence $H(t)$ is both positive definite and conserved locally. By analogy with the inverse-cascade regime in 2D fluid turbulence, we expect that the energy that accumulates at $k_n \simeq k_{\rm tr}$ acts as a source for the direct cascade of H in the range $k_{\rm tr} \ll k_n \ll k_\nu$. To confirm this, we plot, in Fig. 3(a), the flux of H:

$$\Pi_H(k_n) = \left\langle \sum_{j=n}^{N} \Re\left\{ \mathrm{i} k_n^\beta \Phi_j u_j^* \right\} \right\rangle, \tag{8}$$

with $\beta = \log_\lambda(a/c)$. Clearly, as $k_{\rm tr}$ is decreased, the flux increases and tends to flatten for $k_{\rm tr} \ll k_n \ll k_\nu$, suggesting a direct cascade of H. However, the lack of significant separation between $k_{\rm tr}$ and k_ν makes it difficult to identify a range where $\Pi_H(k_n)$ remains constant. In the inset of Fig. 3(a), we plot $\Pi_H(k_n)$ for fixed $k_{\rm tr}$ and different values of ν to observe indeed that, for small viscosities, $\Pi_H(k_n)$ tends to flatten for $k_{\rm tr} \ll k_n \ll k_\nu$. As further confirmation of the direct cascade of H, we show in Fig. 3(b) that, by moving $k_{\rm tr}$ close to k_1, we achieve a large range of constant $\Pi_H(k_n)$. Moreover, in such range, $\mathcal{E}(k_n) \sim k_n^{-\gamma}$ with $\gamma = 2[1+\beta]/3 + 1$ [inset of Fig. 3(b)], as is expected in the direct-cascade regime of H [29].

(b) Large-wave-number forcing. We now address the case $k_f > k_{\rm tr}$ (Table I, runs D; $\mu \neq 0$ helps the system to reach a statistically stationary state but does not contribute to the formation of the condensate [32]). For $k_{\rm tr} = 0$ and with our choice of parameters, $\mathcal{E}(k_n) \sim k_n^{-5/3}$, in the range between the friction-dominated wave numbers and k_f [29]. In this range, $\Pi_E(k_n) < 0$ remains constant and equals the rate of hyperfriction energy dissipation $\epsilon_\mu = \sum_{n=1}^{N} D_\mu(k_n)$. We now consider $k_f > k_{\rm tr} > 0$. Small values of $k_{\rm tr}$ have a negligible effect on energy spectra and fluxes, because at small k_n the inverse energy cascade is already stopped by hyperfriction, so we focus on intermediate values of $k_{\rm tr}$ between k_1 and k_f. For such values of $k_{\rm tr}$, the energy flux [Fig. 4(a)] indicates that the inverse energy cascade is arrested at $k_n \simeq k_{\rm tr}$ and it is accompanied by energy buildup (i.e. the formation of an intermediate-scale condensate) around $k_{\rm tr}$ [Fig. 4(b)].

We see the following two scaling forms on each side of $k_{\rm tr}$: for $k_1 \ll k_n \ll k_{tr}$, $\mathcal{E}(k_n) \sim k_n^{-1}$, which indicates equipartition [Fig. 4(b)], and for $k_{\rm tr} \ll k_n \ll k_f$, $\mathcal{E}(k_n) \sim k_n^{-5/3}$, as we expect in the range of the inverse energy cascade [inset of Fig. 4(b)]. Clearly, the latter range decreases as $k_{\rm tr}$ approaches k_f. The energy transfer that leads to a statistically stationary state is similar to that observed in case (a): the accumulation of energy at scales comparable to $k_{\rm tr}$ is compensated by an increased viscous dissipation at similar scales. Indeed, in Fig. 4(a) we see, together with a peak of dissipation at k_f, a second peak at $k_{\rm tr}$ [33]. Before concluding, we comment on the aforementioned regime of energy equipartition. In shell models, with constant 3D-like coefficients, the wave numbers $k_n \ll k_f$ are isolated from the effects of forcing and viscous damping and the energy flux to these small wave numbers is zero [34]. Therefore, energy in these modes is expected to equilibrate [1,34]. Analogous arguments lead to energy equipartition for $k_n \ll k_{\rm tr}$ in our model: the condensate generated around $k_{\rm tr}$ by the large-k_n inverse cascade indeed acts as a source of energy for the 3D-like low-k_n modes. It remains to be understood whether or not such a regime is expected to persist in real turbulent flows. Energy equipartition

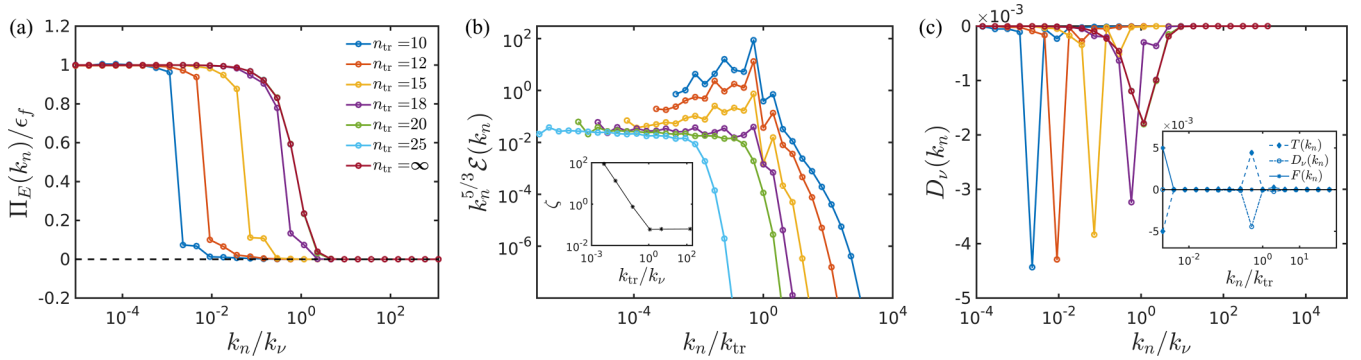

FIG. 2. (a) Log-linear plot of the scaled energy flux versus k_n/k_ν for different values of $n_{\rm tr}$ (runs A0 to A6); the plots for $n_{\rm tr}=20$, 25 are indistinguishable from the $n_{\rm tr}=\infty$ curve. The Kolmogorov wave number corresponds to n lying between 17 and 18. (b) Log-log plots of the compensated energy spectra versus $k_n/k_{\rm tr}$ for the values of $n_{\rm tr}$ in (a) ($k_{\rm tr}=k_0\lambda^{n_{\rm tr}}$); inset: the value of the peak ζ of the compensated spectrum versus $k_{\rm tr}/k_\nu$. (c) Log-linear plot of $D_\nu(k_n)$ versus k_n/k_ν for different values of $n_{\rm tr}$ (runs A); the plots for $n_{\rm tr}=20$, 25 are indistinguishable from the $n_{\rm tr}=\infty$ curve; inset: log-linear plots of $T(k_n)$, $D_\nu(k_n)$, and $F(k_n)$ versus k_n/k_ν for the representative value $n_{\rm tr}=10$. The color coding for $n_{\rm tr}$ is the same in (a)–(c).

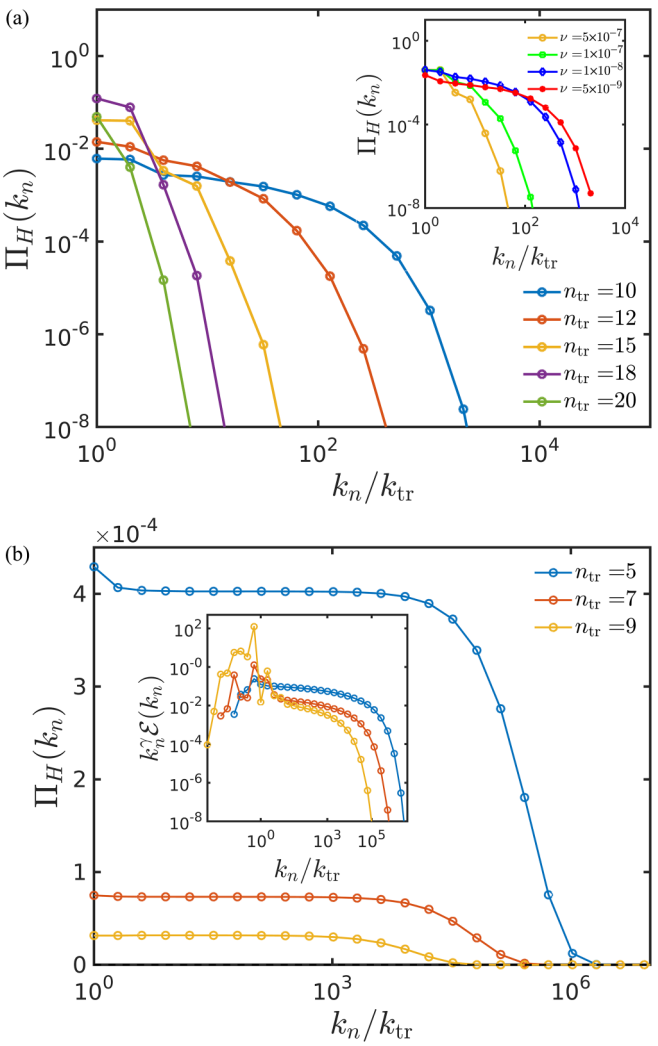

FIG. 3. Log-linear plots of (a) $\Pi_H(k_n)$ versus $k_n/k_{\rm tr}$ for runs A1–A6 and, in the inset, for runs A6, B1, B2, and B3, and (b) for runs C1–C3. Inset of (b): log-log plots of compensated energy spectra versus $k_n/k_{\rm tr}$.

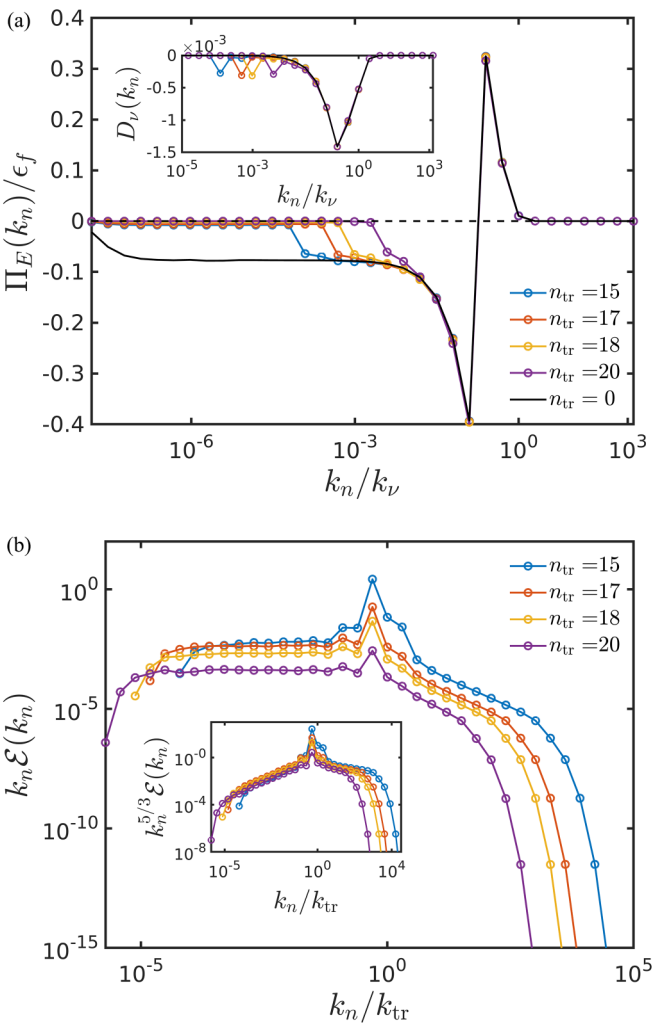

FIG. 4. Plots for runs D1–D5. (a) Log-log plot of the compensated spectra $k_n\mathcal{E}(k_n)$ versus $k_n/k_{\rm tr}$ and in the inset the compensated spectra $k_n^{5/3}\mathcal{E}(k_n)$ versus $k_n/k_{\rm tr}$. (b) Log-linear plots of $\Pi(k_n)$ versus k_n/k_ν and in the inset $D_\nu(k_n)$ versus k_n/k_ν. The Kolmogorov wave number corresponds to n lying between 27 and 28.

at length scales larger than the forcing length scale has been reported in both numerical and experimental investigations [35–37]. However, a recent study [38] has shown that, in 3D homogeneous and isotropic turbulence, the statistics of the large scales is not Gaussian. This has been attributed to a strong coupling between the small and large scales, which may not be captured by shell models. Furthermore, numerical simulations of 3D turbulence have reported significant deviations from the equilibrium spectrum for certain forcing choices [36,39]. Therefore, we expect that spatial and temporal features of the intermediate-scale condensate, specific to the hydrodynamical PDEs, are detrimental to the presence of equipartition at large length scales.

Conclusions. Our study identifies a general energy-transfer mechanism for the nondissipative arrest of energy cascades (inverse or direct) when 3D turbulent dynamics, at small k, coexists with 2D turbulent dynamics, at large k. The shell-model approach we employ allows us to resolve a large range of wave numbers; this is crucial for uncovering the subtle interplay between the nonlinear and viscous terms. Specifically, we find that, when $k_{\rm tr}/k_f > 1$, the direct energy cascade for $k_n < k_{\rm tr}$ is arrested by the 2D-like dynamics at $k_n > k_{\rm tr}$. In contrast, when $k_{\rm tr}/k_f < 1$, the inverse energy cascade for $k_n > k_{\rm tr}$ is arrested by the 3D-like dynamics at $k_n < k_{\rm tr}$. In both cases, the arrest close to $k_{\rm tr}$ results in energy accumulation around $k_{\rm tr}$. In a spatially extended system, such an accumulation of energy would lead to the emergence of spatial structures, or condensates, of size $k_{\rm tr}^{-1}$. A statistically stationary state stems from an increased viscous dissipation, at wave numbers close to $k_{\rm tr}$, which compensates for the energy accumulation. This is reminiscent of condensates in 2D turbulence. Furthermore, we show that, when $k_{\rm tr}/k_f > 1$, the energy that accumulates near to $k_{\rm tr}$ generates a direct cascade of generalized enstrophy for $k_n > k_{\rm tr}$, whereas, when $k_{\rm tr}/k_f < 1$, the modes with $k_n < k_{\rm tr}$ are in statistical equilibrium.

The details of the transitional scale will vary with different models, but the energy-transfer mechanisms we have identified are general and apply to any turbulent system with 2D-like large-k dynamics and 3D-like small-k dynamics. Thus our results will stimulate the study of new physical systems with cascade arrests leading to intermediate-scale condensates.

Acknowledgments. This work was supported in part by the French government through the UCA$^{\rm JEDI}$ Investments in the Future project managed by the National Research Agency (ANR), with Reference No. ANR-15-IDEX-01, and by the International Centre for Theoretical Sciences (ICTS) for the online program Turbulence: Problems at the Interface of Mathematics and Physics (Code No. ICTS/TPIMP2020/12). K.V.K. thanks Laboratoire J. A. Dieudonné of Université Côte d'Azur for hospitality. R.P. and K.V.K. acknowledge support from SERB and NSM (India) and thank SERC (IISc) for computational resources. K.V.K. and D.V. are thankful to S. Mukherjee for useful discussions. D.V. acknowledges support from the International Centre for Theoretical Sciences (ICTS-TIFR), Bangalore, India.

[1] U. Frisch, *Turbulence: The Legacy of A. N. Kolmogorov* (Cambridge University Press, Cambridge, UK, 1995).
[2] G. Boffetta and R. E. Ecke, Two-dimensional turbulence, Annu. Rev. Fluid Mech. **44**, 427 (2012).
[3] R. Pandit, D. Banerjee, A. Bhatnagar, M.-E. Brachet, A. Gupta, D. Mitra, P. P. N. Pal, S. Ray, V. Shukla, and D. Vincenzi, An overview of the statistical properties of two-dimensional turbulence in fluids with particles, conducting fluids, fluids with polymer additives, binary-fluid mixtures, and superfluids, Phys. Fluids **29**, 111112 (2017).
[4] U. Frisch, A. Pomyalov, I. Procaccia, and S. S. Ray, Turbulence in noninteger dimensions by fractal Fourier decimation, Phys. Rev. Lett. **108**, 074501 (2012).
[5] A. Alexakis and L. Biferale, Cascades and transitions in turbulent flows, Phys. Rep. **767-769**, 1 (2018).
[6] M. Verma, *Energy Transfers in Fluid Flows* (Cambridge University Press, Cambridge, UK, 2019).
[7] A. Pouquet, D. Rosenberg, J. E. Stawarz, and R. Marino, Helicity dynamics, inverse, and bidirectional cascades in fluid and magnetohydrodynamic turbulence: A brief review, Earth Space Sci. **6**, 351 (2019).
[8] B. Legras, B. Villone, and U. Frisch, Dispersive stabilization of the inverse cascade for the Kolmogorov flow, Phys. Rev. Lett. **82**, 4440 (1999).
[9] S. Sukoriansky, N. Dikovskaya, and B. Galperin, On the arrest of inverse energy cascade and the Rhines scale, J. Atmos. Sci. **64**, 3312 (2007).
[10] A. van Kan, B. Favier, K. Julien, and E. Knobloch, Spontaneous suppression of inverse energy cascade in instability-driven 2-D turbulence, J. Fluid Mech. **952**, R4 (2022).
[11] G. Miloshevich, D. Laveder, T. Passot, and P.-L. Sulem, Inverse cascade and magnetic vortices in kinetic Alfvén-wave turbulence, J. Plasma Phys. **87**, 905870201 (2021).
[12] S. J. Benavides, K. J. Burns, B. Gallet, J. Y.-K. Cho, and G. R. Flierl, Inverse cascade suppression and shear-layer formation in magnetohydrodynamic turbulence subject to a guide field and misaligned rotation, J. Fluid Mech. **935**, A1 (2022).
[13] M. Linkmann, G. Boffetta, M. C. Marchetti, and B. Eckhardt, Phase transition to large scale coherent structures in two-dimensional active matter turbulence, Phys. Rev. Lett. **122**, 214503 (2019).
[14] N. B. Padhan, K. V. Kiran, and R. Pandit, Novel turbulence and coarsening arrest in active-scalar fluids, Soft Matter **20**, 3620 (2024).
[15] X. M. de Wit, M. Fruchart, T. Khain, F. Toschi, and V. Vitelli, Pattern formation by turbulent cascades, Nature (London) **627**, 515 (2024).
[16] T. Bohr, M. H. Jensen, G. Paladin, and A. Vulpiani, *Dynamical Systems Approach to Turbulence* (Cambridge University Press, Cambridge, UK, 1998).
[17] A. Basu, A. Sain, S. K. Dhar, and R. Pandit, Multiscaling in models of magnetohydrodynamic turbulence, Phys. Rev. Lett. **81**, 2687 (1998).

[18] L. Biferale, Shell models of energy cascade inturbulence, Annu. Rev. Fluid Mech. **35**, 441 (2003).
[19] F. Plunian, R. Stepanov, and P. Frick, Shell models of magnetohydrodynamic turbulence, Phys. Rep. **523**, 1 (2013).
[20] X. M. de Wit, G. Ortali, A. Corbetta, A. A. Mailybaev, L. Biferale, and F. Toschi, Extreme statistics and extreme events in dynamical models of turbulence, Phys. Rev. E **109**, 055106 (2024).
[21] A. A. Mailybaev, Hidden scale invariance of intermittent turbulence in a shell model, Phys. Rev. Fluids **6**, L012601 (2021).
[22] L. Biferale, A. A. Mailybaev, and G. Parisi, Optimal subgrid scheme for shell models of turbulence, Phys. Rev. E **95**, 043108 (2017).
[23] C. J. Miles and C. R. Doering, A shell model for optimal mixing, J. Nonlin. Sci. **28**, 2153 (2018).
[24] R. Benzi, I. Castaldi, F. Toschi, and J. Trampert, Self-similar properties of avalanche statistics in a simple turbulent model, Philos. Trans. R. Soc. A **380**, 20210074 (2022).
[25] G. Boffetta, F. De Lillo, and S. Musacchio, Shell model for quasi-two-dimensional turbulence, Phys. Rev. E **83**, 066302 (2011).
[26] A. Celani, S. Musacchio, and D. Vincenzi, Turbulence in more than two and less than three dimensions, Phys. Rev. Lett. **104**, 184506 (2010).
[27] S. Musacchio and G. Boffetta, Split energy cascade in turbulent thin fluid layers, Phys. Fluids **29**, 111106 (2017).
[28] V. S. L'vov, E. Podivilov, A. Pomyalov, I. Procaccia, and D. Vandembroucq, Improved shell model of turbulence, Phys. Rev. E **58**, 1811 (1998).
[29] T. Gilbert, V. S. L'vov, A. Pomyalov, and I. Procaccia, Inverse cascade regime in shell models of two-dimensional turbulence, Phys. Rev. Lett. **89**, 074501 (2002).
[30] D. Pisarenko, L. Biferale, D. Courvoisier, U. Frisch, and M. Vergassola, Further results on multifractality in shell models, Phys. Fluids **5**, 2533 (1993).
[31] C. K. Chan, D. Mitra, and A. Brandenburg, Dynamics of saturated energy condensation in two-dimensional turbulence, Phys. Rev. E **85**, 036315 (2012).
[32] We have repeated runs D2–D5 with $\mu = 0$ and the conclusions remain the same.
[33] We have checked that the contribution of hyperfriction to the formation of the energy condensate is negligible.
[34] N. Cocciaglia, M. Cencini, and A. Vulpiani, Nonequilibrium statistical mechanics of the turbulent energy cascade: Irreversibility and response functions, Phys. Rev. E **109**, 014113 (2024).
[35] V. Dallas, S. Fauve, and A. Alexakis, Statistical equilibria of large scales in dissipative hydrodynamic turbulence, Phys. Rev. Lett. **115**, 204501 (2015).
[36] A. Alexakis and M.-E. Brachet, On the thermal equilibrium state of large-scale flows, J. Fluid Mech. **872**, 594 (2019).
[37] J.-B. Gorce and E. Falcon, Statistical equilibrium of large scales in three-dimensional hydrodynamic turbulence, Phys. Rev. Lett. **129**, 054501 (2022).
[38] M. Ding, J.-H. Xie, and J. Wang, Departure from the statistical equilibrium of large scales in forced three-dimensional homogeneous isotropic turbulence, J. Fluid Mech. **984**, A71 (2024).
[39] D. Hosking and A. Schekochihin, Emergence of long-range correlations and thermal spectra in forced turbulence, J. Fluid Mech. **973**, A13 (2023).